International Journal of Solids and Structures 129 (2017) 135–145

Contents lists available at ScienceDirect

International Journal of Solids and Structures

journal homepage: www.elsevier.com/locate/ijsolstr

Large deflections of a clamped-slider-pinned rod with uniform intrinsic curvature

V.G.A. Goss*, P. Singh, R. Chaouki

School of Engineering, London South Bank University, London SE1OAA, United Kingdom

ARTICLE INFO

Article history:
Received 4 May 2017
Revised 20 July 2017
Available online 12 September 2017

Keywords:
Intrinsic curvature
Elastica
Rods
Elliptic integrals
Experiments
Loop formation

ABSTRACT

This paper examines large planar deflections of a slender elastic rod with uniform intrinsic curvature, which is clamped at one end and the other end is pinned to a slider allowing it to move freely in the vertical direction as the ends are displaced horizontally in a straight line. The analysis encompasses force-displacement loading paths and corresponding configurations, with a particular focus on the formation of loops. The analysis is accompanied with data obtained from experiments on nickel titanium alloy strips, demonstrating a good match with theoretical predictions.

1. Introduction

Whilst the planar equilibrium of intrinsically straight rods have been subjected to considerable analysis there have been very few studies of intrinsically curved rods. Consequently, our understanding of the effects of intrinsic curvature remains relatively poor. This paper aims to contribute towards redressing that.

We remark here that few rod-like structures, whether artificial or naturally occurring, are actually straight, they nearly all contain a certain amount of intrinsic curvature. Indeed, preliminary studies of animal vibrissae suggest that intrinsic curvature may be advantageous to animals because it generates correspondingly large forces and bending moments at the vibrissal base (Quist and Hartmann, 2012). Deeper understanding of the effects of curvature can assist engineers in devising new technologies that are inspired by nature, for example robotics engineers developing robots that use flexible rods to gather information and explore spaces where light is restricted or too bright (H.Evans et al., 2014; Pearson et al., 2007). Problems involving intrinsically curved rods arise in a variety of real world scenarios; for example when unwinding cable or wire from a spool. It also arises when intrinsically curved rod-like structures, such as textile fibres are bent (González and Lorca, 2004).

The problem of an intrinsically curved rod has been analysed by Love (1892), Frisch-Fay (1962), Snowdon (1963), Fichter and Pinson (1989), and González and Lorca (2004). Love examines the problem of an intrinsically curved rod that is loaded by an end moment. He concludes that the only way in which it affects the problem, compared to the intrinsically straight rod is that "the terminal couple required to hold the wire in the form of a given elastica is diminished by the terminal couple that would be required to bend a naturally straight wire into the given originally circular form" (Love, 1892). However, he does not discuss the problem of an intrinsically curved rod loaded solely by an applied end force. That problem was examined by Frisch-Fay who writes the solutions to the problem in terms of elliptic integrals (Frisch-Fay, 1962). He alludes to an issue that crops up with respect to the elliptic parameter. He noticed that small adjustments in the value of the end force can cause dramatic changes in the value of the elliptic parameter. The net effect is that the distinction between inflectional and noninflectional elastica, which is clear in the case of an intrinsically straight rod, become muddled. Snowdon also analyses the problem in terms of elliptic integrals (Snowdon, 1963). He classifies the solutions into three 'types' according to the value of the elliptic parameter. His paper contains some plots of the shapes of the elastica for the three types. However, his classification has little bearing on how the end load affects those shapes. Fichter and Pinson examine the problem of an eccentrically applied end force (Fichter and Pinson, 1989). Rather than elliptic integrals, they express the solutions in 'raw' integral form (not elliptic integrals) and use a numerical scheme to obtain a relation between the applied end force and the end displacement. González and Lorca also examine the problem (González and Lorca, 2004). They solve the problem in terms of incomplete elliptic integrals numerically for

* Corresponding author at: Dynamics and Solid Mechanics, School of Engineering, London South Bank University, London SE1OAA, United Kingdom.
E-mail address: gossga@lsbu.ac.uk (V.G.A. Goss).

http://dx.doi.org/10.1016/j.ijsolstr.2017.09.006
0020-7683/

certain pairs of values of end force and end displacement and then determine a polynomial fit for the force as a function of the end displacement. However they only consider the configuration of the rod under action of an axially applied end force acting in one direction and they do not examine loop formation.

Although our concern here is restricted to planar equilibrium states, we mention studies involving elastic rods with intrinsic curvature that deform spatially i.e., where twist plays a role. For example, Champneys et al.describe a twisted equilibrium deformation whereby a one twist-per-helical wave configuration arises (Champneys et al., 1997). The authors additionally note that, in the case of spatial deformations, initial curvature breaks complete integrability (though that does not carry across to the planar case). Starotsin et al.consider the problem of successively removing the loops in a helical spring under an end load (Starostin and van der Heijden, 2009). They find that the loops tend not to unwind when pulled, but deform into localised 'hockles' that pop-out one after the other as the end load is increased. Their analysis encompasses planar configurations as well as three-dimensional ones. The planar solutions are given in terms of elliptic integrals and elliptic functions, and arise from zero-moment boundary conditions.

Just as the simplicity of an intrinsically straight rod establishes a basis for practically all analytical studies of rod-like structures, this paper examines the particular case of an intrinsically uniformly curved rod. The rod is clamped at one end and the other end is pinned to a slider allowing it to move freely in the vertical direction as the ends are displaced horizontally in a straight line i.e., rigid loading along the horizontal axis only. That procedure may be referred to as semi-rigid loading. We use a combination of analysis and numerical methods to compute force-displacement diagrams and equilibrium shapes of the rod. The results are compared to experimental data obtained from a series of experiments on nickel titanium strips with appropriate intrinsic curvature. Our analysis encompasses the phenomenon of loop formation, which arises in a range of engineering applications; in his classic book on cable-buoy systems, Berteaux remarked that kinks are the 'mortal enemy of wire ropes' and noted that they are initiated by loop formation (Berteaux, 1976). They also arise in the textile industry (Ramgulam, 2011) and in cable laying activities (Coyne, 1990). However, all the aforementioned studies are restricted to intrinsically straight rods.

2. Formulation of the boundary value problem

2.1. Geometry of the unstressed rod

Consider a rod that has uniform intrinsic curvature $\frac{1}{R}$ i.e., it is an arc of a circle with radius R, see the left hand illustration in Fig. 1. The rod has length $L = R\gamma_i$, where γ_i is the centre angle of the arc. The arc length is parameterised by the variable S, with end points $S = 0$ and $S = L$, i.e., $0 \le S \le L$, where $S = 0$ is the origin of a Cartesian coordinate system (X, Y).

In the case of the unstressed rod, the angle measured anticlockwise from the X axis is denoted $\Psi_i(S)$, as shown in the right hand figure in Fig. 1, where the suffix 'i' denotes the initial unstressed state. In this paper, the intrinsic curvature is positive. Inspection of Fig. 1 indicates that the coordinates $(X_i(S), Y_i(S))$ are given as $X_i(S) = R\sin\Psi_i(S)$, $Y_i(S) = R(1-\cos\Psi_i(S))$ and that

$$\frac{dY_i(S)}{dX_i(S)} = \frac{X_i(S)}{R - Y_i(S)} = \tan\Psi_i(S) \tag{1}$$

and

$$\gamma_i = \arctan\left(\frac{X_i(L)}{R - Y_i(L)}\right) = \arcsin\left(\frac{X_i(L)}{R}\right). \tag{2}$$

2.2. Geometry of the bent rod and experimental set-up

The configuration of the unstressed rod is its reference configuration. The end $S = 0$ is clamped and the end $S = L$ is pinned in a vertical slider, see the experimental set-up shown in Fig. 2. We consider the configuration of the rod when the end $S = L$ is displaced in a straight horizontal line along the X axis by amount D. For each rigid displacement D, the end $S = L$ is free to move vertically along the Y axis. Displacement by amount D can either be in the positive X direction whereby the force in the rod is positive, or in the negative X direction whereby the force is negative, see Fig. 3. In the experiment the end force T is recorded at intervals of D. All measurements of forces reported in this paper are in the range from -0.5 to 1 N. The transducer used to measure the forces has a sensitivity of 0.0001 N. This semi-rigid loading arrangement is specified by the following boundary conditions

$$X(0) = 0, \tag{3}$$

$$Y(0) = 0, \tag{4}$$

$$\Psi(0) = 0, \tag{5}$$

$$X(L) = R\sin\gamma_i + D, \tag{6}$$

$$\frac{d\Psi(L)}{dS} = \frac{1}{R}, \tag{7}$$

where $-L - R\sin\gamma_i \le D \le L - R\sin\gamma_i$. Note that Eqs. (3)–(5) state that the rod is anchored at the origin by clamps. Eq. (6) specifies the rigid loading with respect to the horizontal axis and Eq. (7) states that the curvature at the end $S = L$ is the intrinsic curvature $\frac{1}{R}$. For the purpose of experiments we use uniformly intrinsically curved nickel titanium rods of length L ranging between $300 - 400$mm and flexural rigidity $EI = 0.0034$ Nm^2, where the constants E and I are the modulus of elasticity and the second moment of area respectively. Each rod has a rectangular cross section with a width of 3mm, a thickness of 0.5mm. We assume that those rods (strips) are homogeneous, incompressible, inextensible and that the following linear constitutive relation between bending moment $M(S)$ and curvature $\frac{d\Psi}{dS}$ applies:

$$M = EI\left(\frac{d\Psi}{dS} - \frac{1}{R}\right). \tag{8}$$

During the aforementioned semi-rigid loading sequence the force T acts in the line of action parallel with the X axis. Note that the force is conserved throughout the rod. i.e.,

$$\frac{dT}{dS} = 0. \tag{9}$$

The application of this force sets up a bending moment M, such that

$$\frac{dM}{dS} = T\frac{dY}{dS}. \tag{10}$$

The geometry of deformation of the bent rod is given by the following first order ordinary differential equations

$$\frac{dX}{dS} = \cos\Psi, \tag{11}$$

$$\frac{dY}{dS} = \sin\Psi. \tag{12}$$

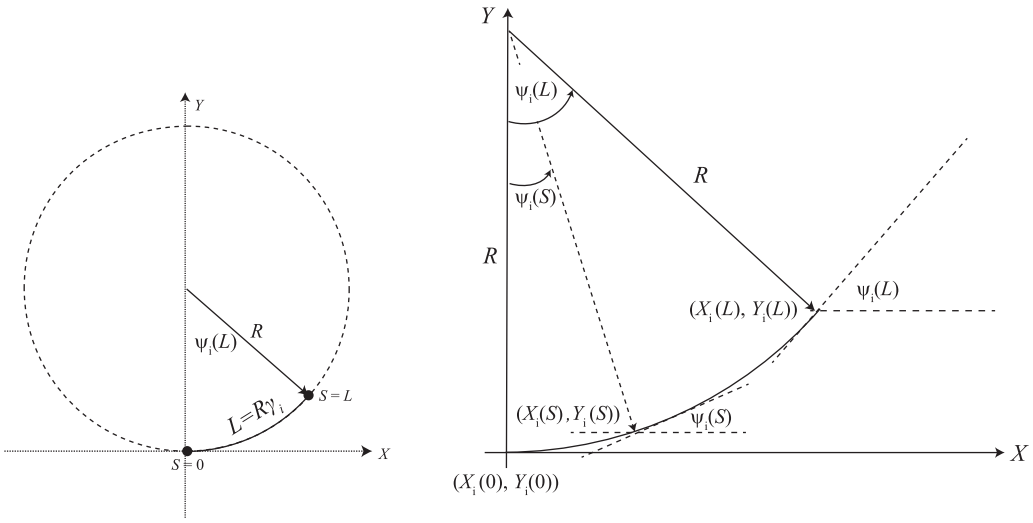

Fig. 1. The rod in its natural unstressed state has uniform intrinsic curvature, i.e., it is an arc of a circle.

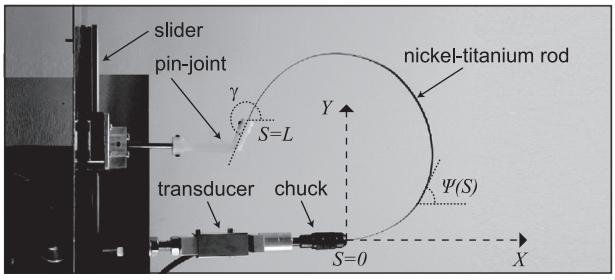

Fig. 2. Photograph of the experimental rig used for the experiments, with coordinates superimposed. Note the rod is clamped at $S = 0$ in a chuck and fixed in a bespoke slider pin-joint at $S = L$ which allows the end to slide freely up and down parallel with the Y axis for each rigid displacement D along the X axis.

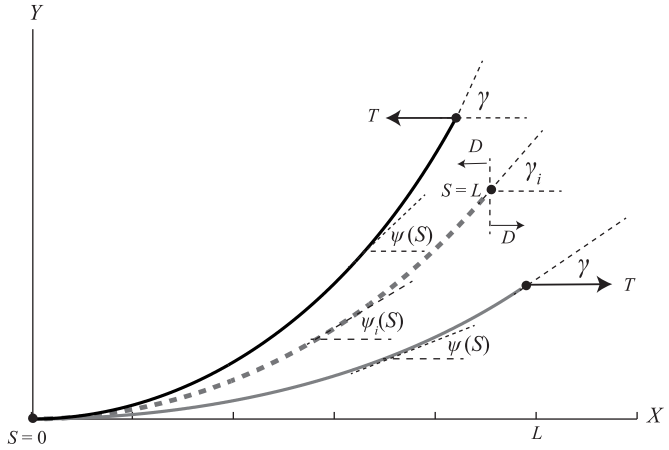

Fig. 3. Three configurations, in dimensional coordinates, of an elastic rod of length L with initial curvature $\gamma_i = \pi/4$. The dashed curve denotes its unstressed state, which is the reference configuration. The two solid curves show its subsequent configurations when it is deflected as the end $S = L$ is displaced in a straight line either towards or away from the end $S = 0$ by amount D, involving a corresponding force T.

Finally, using Eqs. (10),(12) and (8) we obtain the following second order ordinary differential equation (ODE),

$$EI\frac{d^2\Psi}{dS^2} - T\sin\Psi = 0. \tag{13}$$

Eq. (13) is the equation for the elastica.

2.3. The non-dimensional form of the problem

For the purposes of analysis it is convenient to non-dimensionalise the variables, as follows;

$$s = \frac{S}{L},\quad x = \frac{X}{L},\quad y = \frac{Y}{L},\quad r = \frac{R}{L},\quad d = \frac{D}{L},\quad t = \frac{TL^2}{EI},\quad m = \frac{ML}{EI}, \tag{14}$$

where $0 \le s \le 1$. Accordingly, in non-dimensional form, the system of Eqs. (13), (9), (11) and (12) are respectively as follows:

$$\frac{d^2\psi}{ds^2} = t\sin\psi, \tag{15}$$

$$\frac{dt}{ds} = 0, \tag{16}$$

$$\frac{dx}{ds} = \cos\psi, \tag{17}$$

$$\frac{dy}{ds} = \sin\psi. \tag{18}$$

2.4. Boundary conditions

In non-dimensional form, the boundary conditions Eqs. (3)–(7) are as follows:

$$x(0) = 0, \tag{19}$$

$$y(0) = 0, \tag{20}$$

$$\psi(0) = 0, \tag{21}$$

$$x(1) = \frac{\sin\gamma_i}{\gamma_i} + d, \tag{22}$$

$$\frac{d\psi(1)}{ds} = \gamma_i, \tag{23}$$

where $-1 - \frac{\sin\gamma_i}{\gamma_i} \le d \le 1 - \frac{\sin\gamma_i}{\gamma_i}$ and

$$\gamma_i = \frac{1}{r}. \tag{24}$$

The second order ODE Eq. (15) and the three first order odes Eqs. (16)–(18), together with the boundary conditions Eqs. (19)–(23) constitute a well posed system of equations.

3. Solution of the boundary value problem

3.1. First integral

Integrating Eq. (15) we obtain:

$$\frac{1}{2}\left(\frac{d\psi}{ds}\right)^2 + t\cos\psi = \text{constant}. \tag{25}$$

To evaluate the constant in Eq. (25), we apply the boundary condition given by Eq. (23), and we find

$$\text{constant} = \frac{1}{2}\gamma_i^2 + t\cos\gamma \tag{26}$$

where the angle γ is defined as

$$\gamma := \psi(1). \tag{27}$$

It follows from Eqs. (25) and (26) that

$$\left(\frac{d\psi}{ds}\right)^2 = \gamma_i^2 - 2t(\cos\psi - \cos\gamma). \tag{28}$$

Note that, with respect to Eq. (28), we only consider the $+ve$ square root because a rod which has positive initial curvature γ_i (intrinsically curved upwards $\smile$ 'sagging'), cannot be bent into a configuration with negative curvature (downwards $\frown$, 'hogging') under the semi-rigid loading sequence specified for this problem; i.e., under the action of a rigid displacement of the end $s = 1$ by amount d applied horizontally from the reference configuration and in accordance with the boundary conditions Eqs. (19)–(23).

Following rearrangement of Eq. (28) we obtain

$$\frac{d\psi}{ds} = \left(\gamma_i^2 - 4tk^2 + 4t\sin^2\frac{\psi}{2}\right)^{\frac{1}{2}}, \tag{29}$$

where we have used $\cos\psi \equiv 1 - 2\sin^2\frac{\psi}{2}$ and where

$$k := \sin\frac{\gamma}{2}. \tag{30}$$

3.2. Expressions for s, x and y

From Eq. (29) we obtain the following integral

$$s = \int_0^{\psi} \frac{d\theta}{\left(\gamma_i^2 - 4tk^2 + 4t\sin^2\frac{\theta}{2}\right)^{\frac{1}{2}}}. \tag{31}$$

Rewriting Eq. (17) as $dx/ds = \cos\psi \equiv 2\cos^2\frac{\psi}{2} - 1$, we obtain

$$x = 2\int_0^{\psi} \frac{\cos^2\frac{\theta}{2}d\theta}{\left(\gamma_i^2 - 4tk^2 + 4t\sin^2\frac{\theta}{2}\right)^{\frac{1}{2}}} - s. \tag{32}$$

Similarly, expressing Eq. (18) as $dy/ds = \sin\psi \equiv 2\sin\frac{\psi}{2}\cos\frac{\psi}{2}$, we obtain

$$y = \frac{1}{t}\left(\left(\gamma_i^2 - 4tk^2 + 4t\sin^2\frac{\psi}{2}\right)^{\frac{1}{2}} - \left(\gamma_i^2 - 4tk^2\right)^{\frac{1}{2}}\right). \tag{33}$$

3.3. The elliptic parameter

When formulating Eqs. (31)–(33) in terms of elliptic integrals, as listed in the Appendix, the elliptic parameter p^2 needs to be introduced. This is defined as:

$$p^2 := k^2 - \frac{\gamma_i^2}{4t}. \tag{34}$$

At an inflection point $\frac{d\psi}{ds} = 0$ must hold. This condition together with equation Eq. (29) implies that

$$\sin^2\frac{\psi}{2} = p^2. \tag{35}$$

Clearly Eq. (35) is only true for $0 \le p^2 \le 1$. When $p^2 < 0$ or $p^2 > 1$ we have a contradiction in Eq. (35) and therefore conclude that $\frac{d\psi}{ds} \neq 0$ i.e., an inflection point does not exist. Thus, the existence of inflection points can be determined from the value of the elliptic parameter p^2. For the case $t < 0$, both $p^2 \le 1$ and $p^2 > 1$ are allowed in Eq. (34). Therefore, for $t < 0$ we can have both inflectional ($p^2 \le 1$) and noninflectional ($p^2 > 1$) solutions. These correspond to Snowdon's solutions of the "First Type" and "Second Type", respectively. In the case of $t > 0$ we have $p^2 < 0$. Thus Eq. (35) breaks down and therefore the condition it is derived from ($\frac{d\psi}{ds} = 0$) cannot be true. In which case $\frac{d\psi}{ds} \neq 0$ must hold and solutions are noninflectional. These correspond to Snowdon's solutions of the "Third Type" (Snowdon, 1963). We remark here that Snowdon describes his Types of solutions in terms of compression (First and Second Types) and tension (Third Type). However, whether or not a rod is under compression or tension depends on the values of γ_i and d as well as t.

We make some remarks on the elliptic parameter p^2 given by Eq. (34) and elliptic integrals.

- For a given $\gamma_i \neq 0$, p^2 depends explicitly on the force t. This is not the case for the straight rod.
- The force t does not factor out neatly from the elliptic integrals as is the case for the straight rod. This means that the solutions, whether in our raw integral form (Eqs. (31)–(33)) or elliptic integral form (see Appendix), must be solved numerically to determine t and γ.
- In the case $t < 0$, for a given $\gamma_i \neq 0$, we don't know if $p^2 \le 1$ or $p^2 > 1$, since we need to know t and γ to determine p^2, and these are not known yet. This makes it difficult to decide which form of the solutions in terms of elliptic integrals (given in the Appendix) to work with to determine t and γ.
- Finally, for $t < 0$, since both $p^2 \le 1$ and $p^2 > 1$ are allowed, there is no reason why not that for a given $\gamma_i \neq 0$ both $p^2 \le 1$ and $p^2 > 1$ can occur. In fact, for $\gamma_i = \frac{\pi}{4}$, Fig. 4 shows this to be the case.

These observations indicate that it is problematic to work with the solutions in elliptic integral form to plot td diagrams and equilibrium shapes. We therefore proceed to work with the solutions to this problem given by Eqs. (31)–(33). Nevertheless, for completeness, the elliptic integral form for the solutions is given in the Appendix.

3.4. Solution for t and γ

Eqs. (31)–(33) can be solved numerically once t and γ are known. Setting $s = 1$, whereby $\psi(1) = \gamma$, Eqs. (31)–(33) become

$$1 = \int_0^{\gamma} \frac{d\theta}{\left(\gamma_i^2 - 4tk^2 + 4t\sin^2\frac{\theta}{2}\right)^{\frac{1}{2}}}, \tag{36}$$

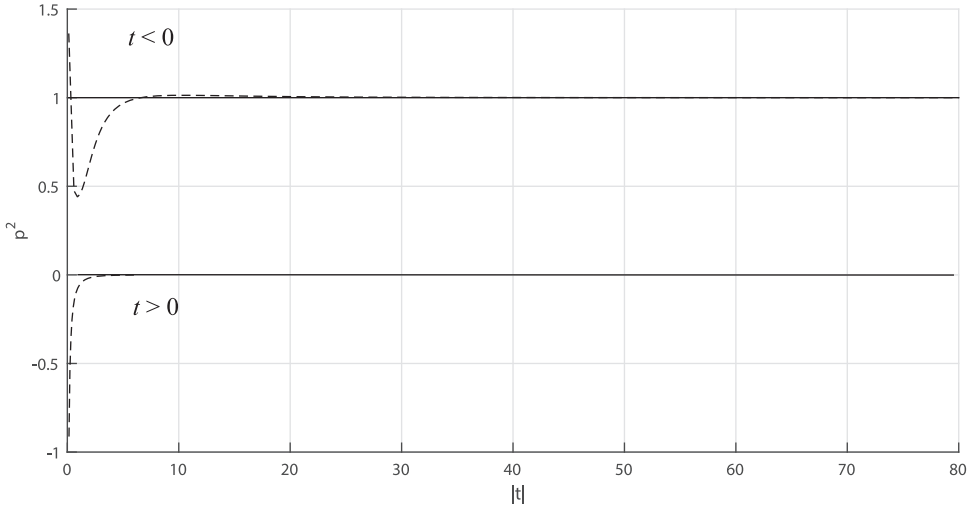

Fig. 4. Plots of p^2 versus the magnitude of the force t, for the cases $t<0$ (top) and $t>0$ (bottom) using Eq. (34) with $\gamma_i = \frac{\pi}{4}$. In the case of $t<0$ it can be seen that p^2 is initially greater than unity corresponding to noninflectional configurations, then drops below unity for a certain domain of t where there are inflectional solutions and then rises above it rendering noninflectional solutions again, but is asymptotic to unity as $|t|$ increases i.e., $p^2 \to 1$ as $|t| \to \infty$. In the case of $t>0$ the rod is always noninflectional because $p^2 < 0$, but is asymptotic to zero as t increases i.e., $p^2 \to 0$ as $t \to \infty$.

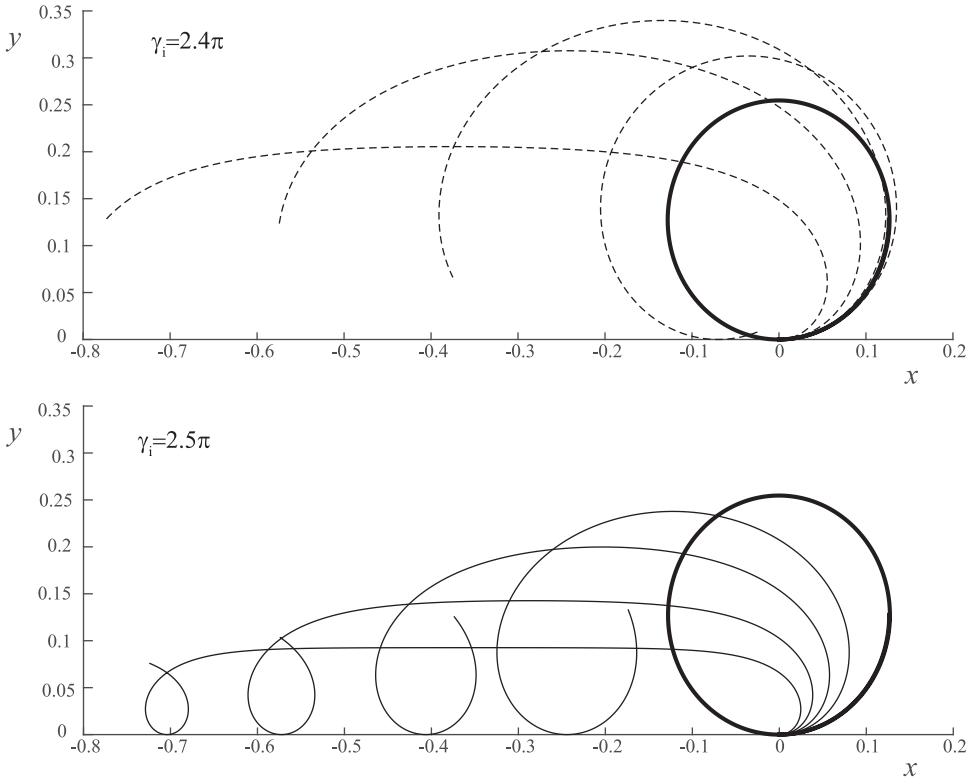

Fig. 5. Configurations of two rods with $\gamma_i = 2.4\pi$ (dashed curves top) and $\gamma_i = 2.5\pi$ (solid curves bottom), deformed with $t<0$ from the natural state (bold curve). Since $2.4\pi < \gamma_1^c$ no loops form and note that γ decreases as the end force is applied. However, since $2.5\pi > \gamma_1^c$ loop formation arises and note that γ increases as the end force is applied.

$$x(1) = 2\int_0^{\gamma} \frac{\cos^2\frac{\theta}{2}d\theta}{\left(\gamma_i^2 - 4tk^2 + \sin^2\frac{\theta}{2}\right)^{\frac{1}{2}}} - 1, \tag{37}$$

$$y(1) = \frac{1}{t}\left(\gamma_i - \left(\gamma_i^2 - 4tk^2\right)^{\frac{1}{2}}\right). \tag{38}$$

To find t and γ we need to simultaneously solve Eqs. (36), (37) together with Eq. (22) i.e.,

$$f(\gamma_i, \gamma, t) := \int_0^{\gamma} \frac{d\theta}{\left(\gamma_i^2 - 4tk^2 + 4t\sin^2\frac{\theta}{2}\right)^{\frac{1}{2}}} - 1 = 0, \tag{39}$$

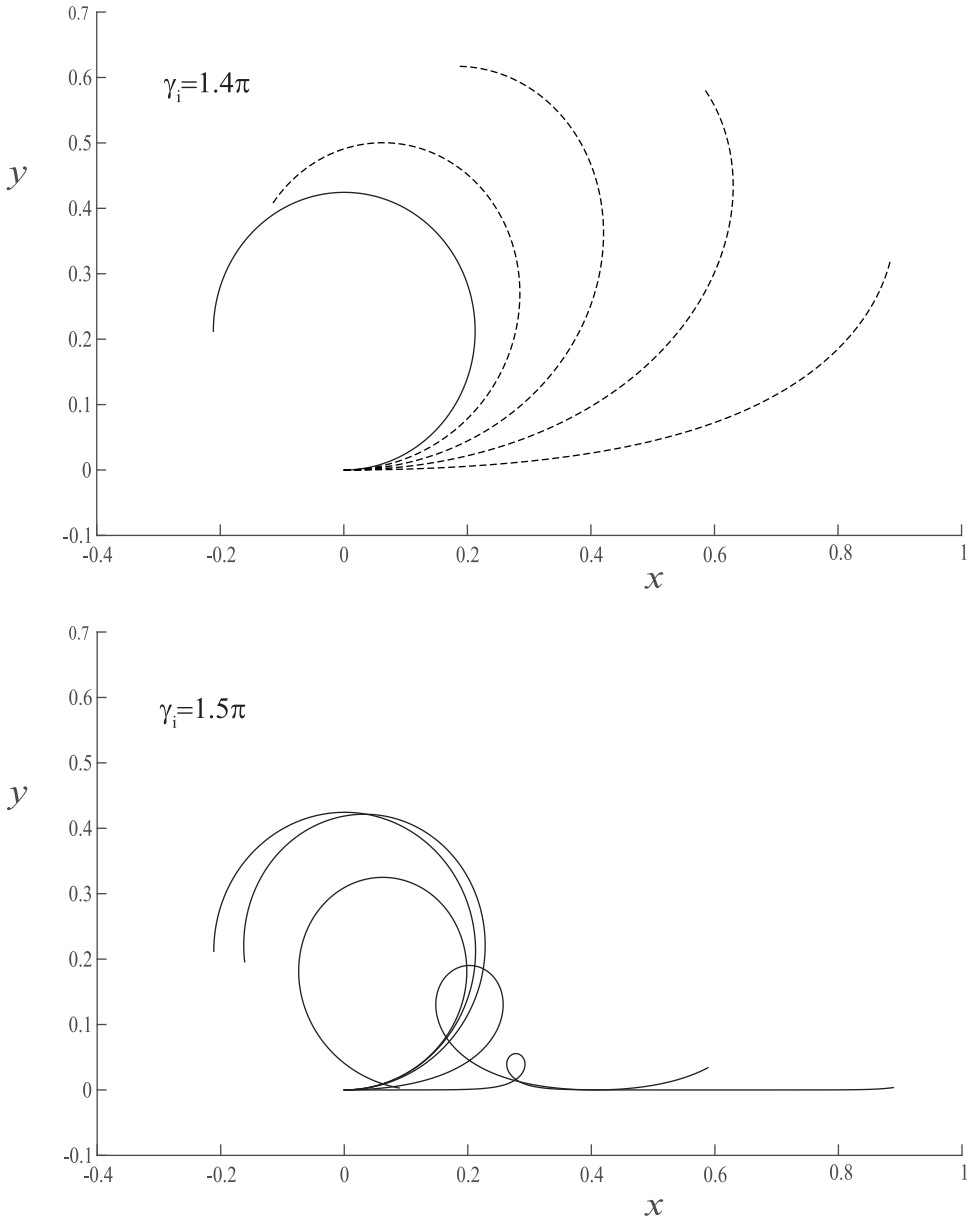

Fig. 6. Configurations of two rods with $\gamma_i = 1.4\pi$ (dashed curves top) and $\gamma_i = 1.5\pi$ (solid curves bottom), deformed with $t > 0$ from the natural state (bold curve). Since $1.4\pi < \gamma_1^c$ no loops form and note that γ decreases as the end force is applied. However, since $1.5\pi > \gamma_1^c$ loop formation arises and note that γ increases as the end force is applied.

and

$$g(\gamma_i, \gamma, t) := 2\int_0^{\gamma} \frac{\cos^2\frac{\theta}{2}d\theta}{\left(\gamma_i^2 - 4tk^2 + 4t\sin^2\frac{\theta}{2}\right)^{\frac{1}{2}}} - 1 - \frac{\sin\gamma_i}{\gamma_i} - d = 0, \tag{40}$$

where we input d and solve for (γ, t) pairs.

We remark here that for the case $\gamma_i = 0$, a straight (inextensible) rod, solving Eqs. (39) and (40) is straightforward because t factorises neatly out of the integrals such that Eqs. (39) and (40) become respectively:

$$f(0, \gamma, t) = \frac{1}{\sqrt{-t}}K(p) - 1 = 0, \tag{41}$$

and

$$g(0, \gamma, t) = \frac{2}{\sqrt{-t}}E(p) - 2 - d = 0, \tag{42}$$

where $p = \sin\frac{\gamma}{2}$ and $K(p)$ and $E(p)$ are the complete elliptic integrals of the first and second kind respectively. For the case $p = 0$ in Eq. (41) we obtain the magnitude of applied end force, denoted t_E, required to buckle a straight rod:

$$t_E := \frac{\pi^2}{4}. \tag{43}$$

Note t_E is also known as the Euler buckling load.

4. Loop formation

4.1. Conditions for loop formation

Careful observations of experiments indicate that, under the semi-rigid loading sequence described by the boundary conditions Eqs. (19)–(23), whereby the end $s = 1$ is displaced by amount d in a continuous line, a loop forms when the angle at the end γ tends to increase, see Figs. 5 and 6. We note here that from

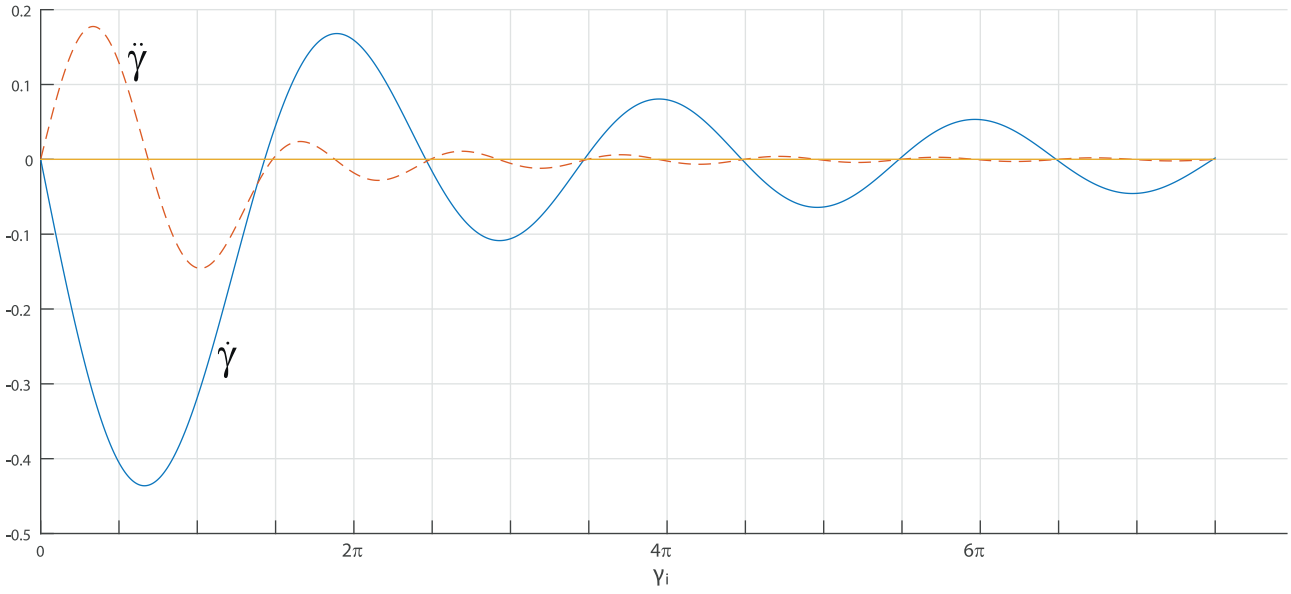

Fig. 7. Plots of $\dot{\gamma}$ and $\ddot{\gamma}$, i.e., Eq. (51) and Eq. (52) respectively. These plots can be used with Eqs. (46) and (47) to determine the critical angles γ_n^c.

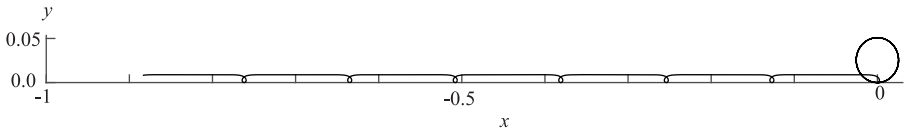

Fig. 8. A rod with $\gamma_i = 12\frac{1}{2}\pi$ deformed into a configuration containing six small knots with $t = -50,000$.

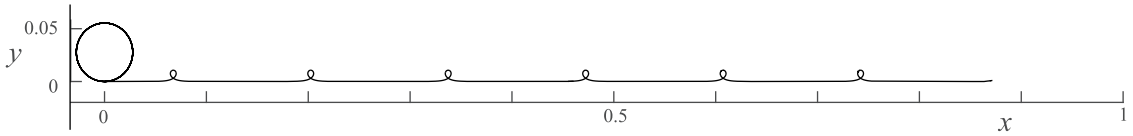

Fig. 9. A rod with $\gamma_i = 11\frac{1}{2}\pi$ deformed into a configuration containing six small knots with $t = 35,000$.

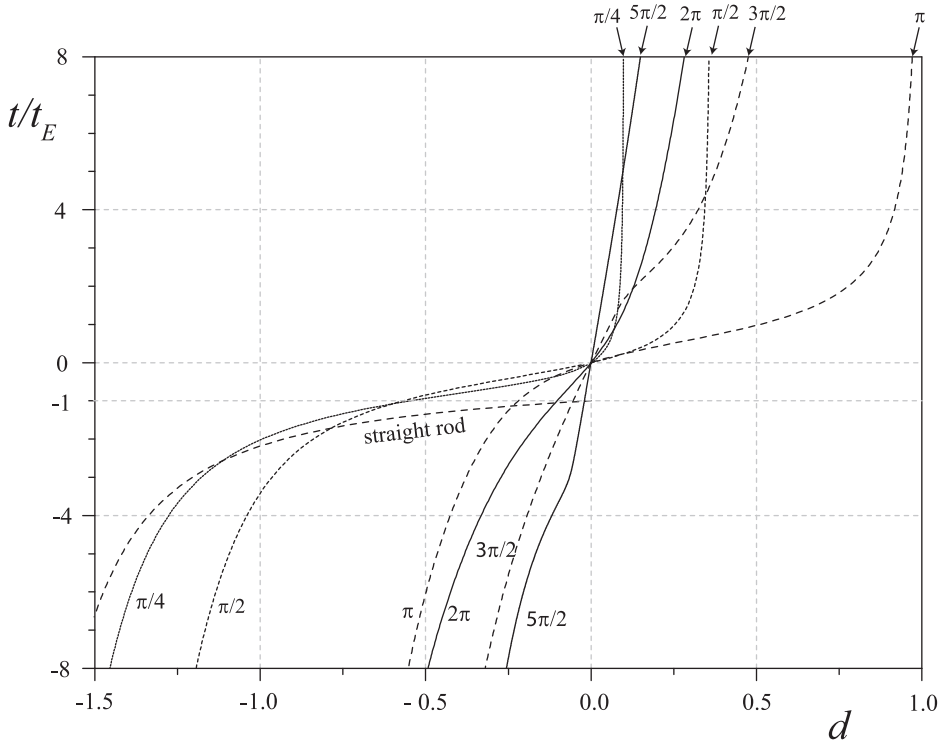

Fig. 10. Plots of td loading paths for a range of γ_i. Note that the straight rod, which buckles at $t/t_E = -1$, has no solutions for $d > 0$ because the rod is inextensible.

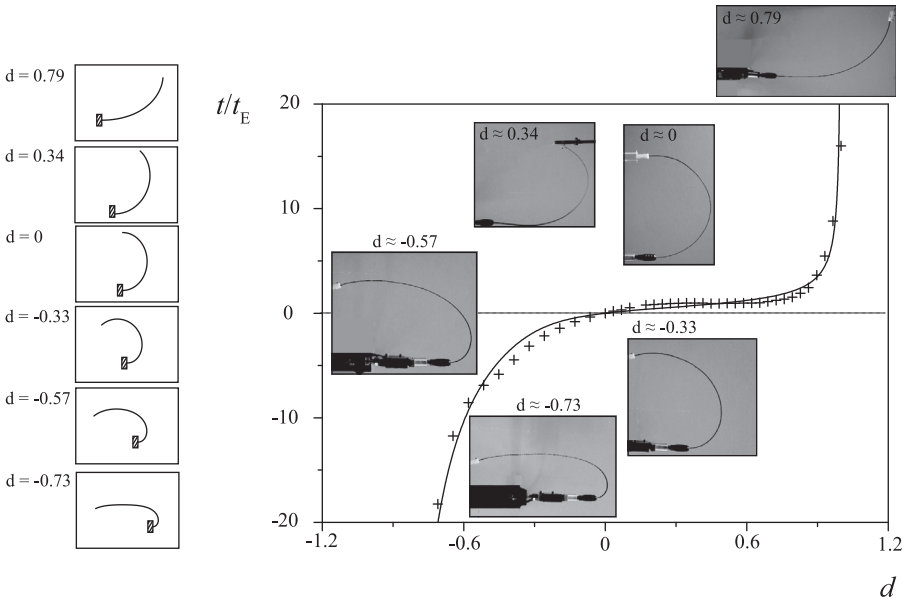

Fig. 11. *td* loading path for a rod with $\gamma_i = 180^\circ$, together with experimental data. Note that no loops arise for either $t < 0$ or $t > 0$, see Table 1.

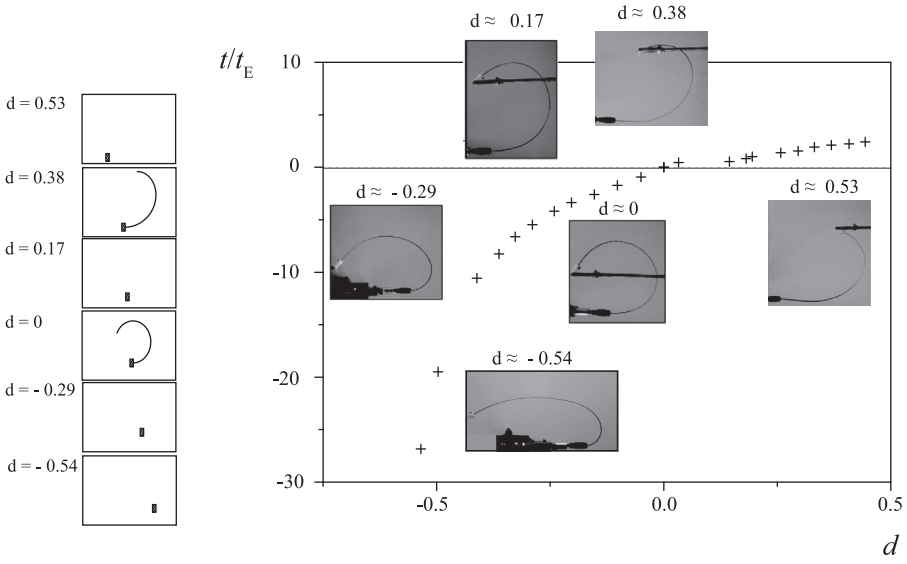

Fig. 12. *td* loading path for a rod with $\gamma_i = 240^\circ$, together with experimental data. Note that no loops arise for either $t < 0$ or $t > 0$, see Table 1.

Eq. (36) changes in t correspond with changes in γ. Consequently, we are justified in stating that $\gamma = \gamma(t)$. For infinitesimally small t, applying a Taylor Series expansion and noting that $\gamma(0) = \gamma_i$, we obtain

$$\gamma(t) = \gamma(0) + \frac{d\gamma(t)}{dt}\Big|_{t=0} t \quad + \quad \frac{1}{2}\frac{d^2\gamma(t)}{dt^2}\Big|_{t=0} t^2 \quad + \quad O(t^3). \quad (44)$$

For convenience we can write

$$\dot{\gamma} := \frac{d\gamma(t)}{dt}\Big|_{t=0} \quad \text{and} \quad \ddot{\gamma} := \frac{d^2\gamma(t)}{dt^2}\Big|_{t=0}. \quad (45)$$

We consider Eq. (44) under rigid loading of d from the unstressed state. For $t < 0$ Eq. (44) indicates that if $\dot{\gamma} > 0$ with t decreasing, $\gamma(t)$ decreases and the rod is pulled straight. For $t > 0$ Eq. (44) indicates that if $\dot{\gamma} < 0$ with t increasing, $\gamma(t)$ decreases and the rod is also pulled straight. For $t < 0$ and $\dot{\gamma} < 0$ with t decreasing, $\gamma(t)$ increases and loops form. Similarly, for $t > 0$ and $\dot{\gamma} > 0$ with t increasing, $\gamma(t)$ increases and loops form.

For the case that $\dot{\gamma} = 0$, we need to examine the term $\ddot{\gamma}$ in Eq. (44). If $\ddot{\gamma} < 0$ with t^2 increasing, then $\gamma(t)$ decreases for all t, in which case the rod is pulled straight. When $\ddot{\gamma} > 0$ with t^2 increasing, then $\gamma(t)$ increases, in which case loops form.

It follows, the conditions for loop formation are:

$$\dot{\gamma} < 0 \quad (t < 0), \qquad \dot{\gamma} > 0 \quad (t > 0) \quad (46)$$

and for all t we have

$$\ddot{\gamma} > 0. \quad (47)$$

4.2. Critical angles for loop formation

Physical reasoning leads us to expect that a loop will only form if the rod is sufficiently 'long' (has large enough γ_i) such that as $|d|$ increases, the end of the rod will self-intersect another point on the rod and form a loop i.e., loop formation can only arise once γ_i exceeds a critical value. More generally, n loops form at critical values denoted by γ_n^c. We now proceed to determine γ_n^c.

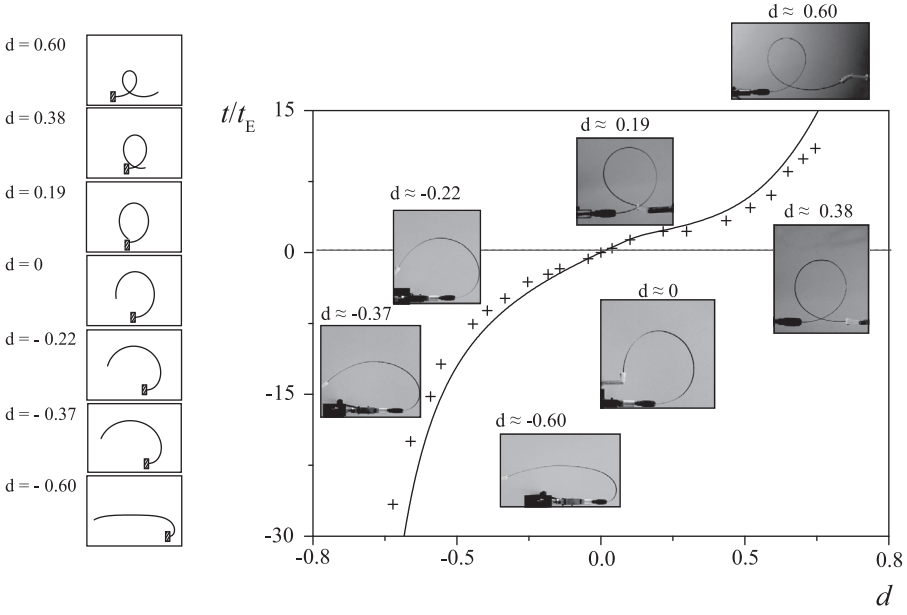

Fig. 13. *td* loading path for a rod with $\gamma_i = 275^\circ$, together with experimental data. Note for $t > 0$ that one loop forms but no loops for $t < 0$, see Table 1.

If there is a function $f(\theta, t)$ that is a continuous and differentiable in both t and θ, then according to Leibniz's Integral Rule

$$\frac{d}{dt}\int_0^{\gamma(t)} f(\theta,t)\, d\theta = \int_0^{\gamma(t)} \frac{\partial f(\theta,t)}{\partial t}\, d\theta + f(\gamma(t),t)\frac{d\gamma(t)}{dt}. \tag{48}$$

Applying Eqs. (48)–(36) (and using $\cos\theta \equiv 1 - 2\sin^2\frac{\theta}{2}$) we obtain

$$\frac{1}{\gamma_i}\frac{d\gamma}{dt} = -\int_0^{\gamma} \frac{\left(\cos\theta - \cos\gamma + t\sin\gamma\frac{d\gamma}{dt}\right)d\theta}{\left[\gamma_i^2 - 2t(\cos\theta - \cos\gamma)\right]^{\frac{3}{2}}}. \tag{49}$$

Additionally, applying Eqs. (48) and (49), we obtain:

$$\frac{d^2\gamma}{dt^2} = -\gamma_i\int_0^{\gamma} d\theta\left[\frac{\left(2\sin\gamma\frac{d\gamma}{dt} + t\cos\gamma\left(\frac{d\gamma}{dt}\right)^2 + t\sin\gamma\frac{d^2\gamma}{dt^2}\right)}{\left(\gamma_i^2 - 2t(\cos\theta - \cos\gamma)\right)^{\frac{3}{2}}}\right.$$
$$\left. + \frac{3\left(\cos\theta - \cos\gamma + t\sin\gamma\frac{d\gamma}{dt}\right)^2}{\left(\gamma_i^2 - 2t(\cos\theta - \cos\gamma)\right)^{\frac{5}{2}}}\right] - \frac{t}{\gamma_i^2}\sin\gamma\left(\frac{d\gamma}{dt}\right)^2. \tag{50}$$

Setting $t = 0$ in Eq. (49) and integrating, we obtain

$$\dot{\gamma} = -\frac{1}{\gamma_i}\left(\frac{1}{\gamma_i}\sin\gamma_i - \cos\gamma_i\right). \tag{51}$$

Similarly, setting $t = 0$ in Eq. (50) and integrating, we obtain the following

$$\ddot{\gamma} = \frac{1}{\gamma_i^2}\left(\frac{9}{4\gamma_i^2} - 1\right)\sin 2\gamma_i - \frac{5}{2\gamma_i^3}\cos 2\gamma_i - \frac{2}{\gamma_i^3}. \tag{52}$$

Plots of Eqs. (51) and (52) are shown in Fig. 7.

For $t < 0$, applying the condition in Eqs. (46)–(51), we find from Fig. 7 that $\gamma_i > 2.4590\pi = 442.63^\circ$. Then applying the condition Eqs. (47)–(52), we find from Fig. 7 that $\gamma_i > 2.4895\pi = 448.12^\circ$. To satisfy both conditions, take $\gamma_1^c = 2.4895\pi = 448.12^\circ$. We remark here that this result is in accordance with what one might expect from physical reasoning i.e, under the action of a negative force one would expect loops to form somewhere in the region $2\pi < \gamma_1^c < 5\pi/2$ i.e., when the rod is sufficiently 'long', as shown in Fig. 5.

Table 1
Table of critical angles for loop formation.

Number of loops n	$\gamma_n^c(t<0)$	$\gamma_n^c(t>0)$
1	$2.4895\pi = 448.12^\circ$	$1.4815\pi = 266.67^\circ$
2	$4.4943\pi = 808.98^\circ$	$3.4927\pi = 628.68^\circ$
3	$6.4961\pi = 1169.30^\circ$	$5.4954\pi = 989.17^\circ$
⋮	⋮	⋮

For $t > 0$, applying the condition in Eqs. (46)–(51), we find from Fig. 7 that $\gamma_i > 1.4303\pi = 257.45^\circ$.Then applying the condition Eqs. (47)–(52), we find from Fig. 7 that $\gamma_i > 1.4815\pi = 266.67^\circ$. In this case, to satisfy both conditions, take $\gamma_1^c = 1.4815\pi = 266.67^\circ$.

4.3. Multi-loop formation

Analysis similar to that of Section 4.2 gives the critical angles for higher numbers of loops, shown in Table 1.

It may be observed that the difference between consecutive critical angles for loop formation is very close to 2π. For $t < 0$:

$$\gamma_2^c - \gamma_1^c = 360.86^\circ$$
$$\gamma_3^c - \gamma_2^c = 360.32^\circ$$
$$\vdots$$

and for $t > 0$:

$$\gamma_2^c - \gamma_1^c = 362.01^\circ$$
$$\gamma_3^c - \gamma_2^c = 360.49^\circ$$
$$\vdots$$

For large t the loops take the form of localised knots, see Figs. 8 and 9.

5. Loading paths: theory and experiments

A set of loading paths for a range of values of d, (where $-1 - \frac{\sin\gamma_i}{\gamma_i} \le d \le 1 - \frac{\sin\gamma_i}{\gamma_i}$), is plotted in Fig. 10 where it can be seen that the end force t has been normalised by dividing by t_E, given by Eq. (43). Note that large forces arise when d approaches

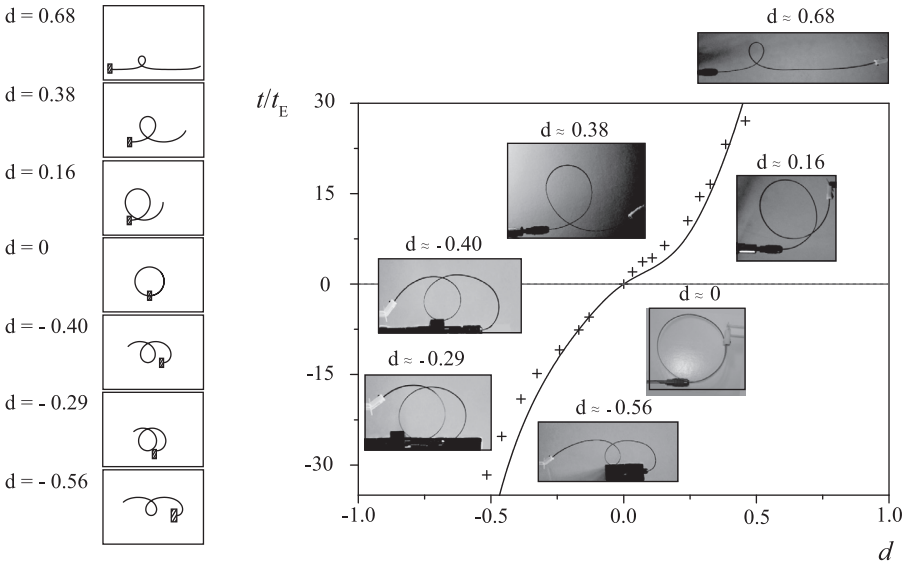

Fig. 14. *td* loading path for a rod with $\gamma_i = 490^\circ$, together with experimental data. Note that one loop forms for both $t < 0$ and $t > 0$, see Table 1.

its lower and upper limits. We additionally provide plots of data obtained from experiments for comparison, see Figs. 11–14. Those plots show the loading paths and accompanying photographs of the configurations of nitinol strips.

6. Conclusions

As pointed out in this paper, the solutions to this boundary value problem, as expressed in terms of elliptic integrals, which are set out in the Appendix, are unwieldy. Nevertheless using Eqs. (31)–(33) we have managed to carry out useful analysis of loop formation. It remains to be seen what can be done with respect to other boundary conditions, different loading sequences and cases where the intrinsic curvature is a function of arc length *s*. Indeed, this paper throws up new questions regarding the loading sequences required to attain inflectional and noninflectional equilibrium configurations; for it is evident that small changes in the boundary conditions and loading sequences can have significant effects on the configuration of the rod, encompassing both inflectional and noninflectional forms.

The experimental data presented here correlates well with that predicted by the theory. That is not a trivial point, for although there is a substantial body of literature and research on rod theory that has contributed to our understanding of the mechanics, perhaps rather too much of that remains of restricted interest due to its failure to demonstrate (rather than simply mention) connections with real world problems. Carefully conducted experiments serve to bridge that gap. We add here that our experiments involve nitinol strips i.e., long slender rods of rectangular cross section with a thickness considerably smaller than the width. These do not deform out of the plane under the experimental procedure followed here. However, for experiments on rods with circular cross sections, out of plane configurations can be observed. The analysis of those requires a three-dimensional spatial elastica model, as opposed to the two-dimensional planar elastica model used here.

Acknowledgement

This research was funded by London South Bank University.

Appendix A. Solutions in terms of Elliptic Integrals

This appendix sets out the solutions for this boundary value problem expressed as Elliptic Integrals. There are three cases for $t < 0$ and one case of $t > 0$.

Elliptic Integral Solutions for $t < 0$

Case 1: $0 < p^2 < 1$

In this case the elliptic argument ϕ is given as:

$$\phi = \arcsin\left(\frac{\sin\frac{\psi}{2}}{p}\right) \tag{53}$$

and

$$s = \frac{1}{\sqrt{-t}}F(\phi, p), \tag{54}$$

$$x = \frac{1}{\sqrt{-t}}(2E(\phi, p) - F(\phi, p)), \tag{55}$$

$$y = \frac{2p}{\sqrt{-t}}(1 - \cos\phi). \tag{56}$$

At $s = 1$, $\psi(1) = \gamma$ and we find the following

$$\phi_\gamma = \arcsin\left(\frac{\sin\frac{\gamma}{2}}{p}\right), \tag{57}$$

$$1 = \frac{1}{\sqrt{-t}}F\left(\phi_\gamma, p\right), \tag{58}$$

$$x(1) = \frac{1}{\sqrt{-t}}\left(2E(\phi_\gamma, p) - F(\phi_\gamma, p)\right), \tag{59}$$

$$y(1) = \frac{2p}{\sqrt{-t}}\left(1 - \cos\phi_\gamma\right). \tag{60}$$

Case 2: $p^2 > 1$

In this case the elliptic argument ϕ is given as:

$$\phi = \frac{\psi}{2} \tag{61}$$

and

$$s = \frac{1}{\sqrt{-t}p}F\left(\phi, \frac{1}{p}\right), \tag{62}$$

$$x = \frac{1}{\sqrt{-t}}\left(2pE\left(\phi, \frac{1}{p}\right) - \frac{2p^2-1}{p}F\left(\phi, \frac{1}{p}\right)\right), \tag{63}$$

$$y = \frac{2p}{\sqrt{-t}}\left(1 - \left(1 - \frac{1}{p^2}\sin^2\phi\right)^{\frac{1}{2}}\right). \tag{64}$$

At $s = 1$, $\psi(1) = \gamma$ and we find the following

$$\phi_\gamma = \frac{\gamma}{2}, \tag{65}$$

$$1 = \frac{1}{\sqrt{-t}p}F\left(\phi_\gamma, \frac{1}{p}\right), \tag{66}$$

$$x(1) = \frac{1}{\sqrt{-t}}\left(2pE\left(\phi_\gamma, \frac{1}{p}\right) - \frac{2p^2-1}{p}F\left(\phi_\gamma, \frac{1}{p}\right)\right), \tag{67}$$

$$y(1) = \frac{2p}{\sqrt{-t}}\left(1 - \left(1 - \frac{1}{p^2}\sin^2\phi_\gamma\right)^{\frac{1}{2}}\right). \tag{68}$$

Case 3: $p^2 = 1$

In this case the elliptic argument ϕ is given as:

$$\phi = \frac{\psi}{2} \tag{69}$$

and

$$s = \frac{1}{\sqrt{-t}}\tanh^{-1}\sin\phi, \tag{70}$$

$$x = \frac{2}{\sqrt{-t}}\left(\sin\phi - \frac{1}{2}\tanh^{-1}\sin\phi\right), \tag{71}$$

$$y = \frac{2}{\sqrt{-t}}(1 - \sin\phi). \tag{72}$$

At $s = 1$, $\psi(1) = \gamma$ and we find the following

$$\phi_\gamma = \frac{\gamma}{2}, \tag{73}$$

$$1 = \frac{1}{\sqrt{-t}}\tanh^{-1}\sin\phi_\gamma, \tag{74}$$

$$x(1) = \frac{2}{\sqrt{-t}}\left(\sin\phi_\gamma - \frac{1}{2}\tanh^{-1}\sin\phi_\gamma\right), \tag{75}$$

$$y(1) = \frac{2}{\sqrt{-t}}\left(1 - \cos\phi_\gamma\right). \tag{76}$$

Elliptic Integral Solutions for $t > 0$

In this case the elliptic parameter is given as:

$$p^2 = k^2 - \frac{\gamma_i^2}{4t} < 0 \tag{77}$$

and for all p^2, the elliptic argument is given as

$$\phi = \frac{\psi}{2}, \tag{78}$$

such that

$$s = \frac{1}{\sqrt{t\left(-p^2\right)}}F\left(\phi, \frac{1}{p}\right), \tag{79}$$

$$x = \frac{2\sqrt{\left(-p^2\right)}}{\sqrt{t}}\left[\frac{2p^2-1}{2p^2}F\left(\phi, \frac{1}{p}\right) - E\left(\phi, \frac{1}{p}\right)\right], \tag{80}$$

$$y = \frac{2\sqrt{\left(-p^2\right)}}{\sqrt{t}}\left[\left(1 - \frac{\sin^2\phi}{p^2}\right)^{\frac{1}{2}} - 1\right]. \tag{81}$$

At $s = 1$, $\psi(1) = \gamma$ and we find the following

$$\phi_\gamma = \frac{\gamma}{2}, \tag{82}$$

$$1 = \frac{1}{\sqrt{t\left(-p^2\right)}}F\left(\phi_\gamma, \frac{1}{p}\right), \tag{83}$$

$$x(1) = \frac{2\sqrt{\left(-p^2\right)}}{\sqrt{t}}\left[\frac{2p^2-1}{2p^2}F\left(\phi_\gamma, \frac{1}{p}\right) - E\left(\phi_\gamma, \frac{1}{p}\right)\right], \tag{84}$$

$$y(1) = \frac{2\sqrt{\left(-p^2\right)}}{\sqrt{t}}\left[\left(1 - \frac{\sin^2\phi_\gamma}{p^2}\right)^{\frac{1}{2}} - 1\right]. \tag{85}$$

We note that solutions are inflectional for $t < 0$ with $p^2 \leq 1$ and noninflectional for $p^2 > 1$. For $t > 0$ all solutions are noninflectional.

References

Berteaux, H., 1976. Buoy Engineering. New York: John Wiley and Sons.

Champneys, A.R., Thompson, J., van der Heijden, G., 1997. Spatially complex localization after one-twist-per-wave equilibria in twisted circular rods with initial curvature. Proc. R. Soc. A Math. Phys. Eng. Sci. 355 (1732), 2298–2312.

Coyne, J., 1990. Analysis of the formation and elimination of loops in twisted cable. IEEE J. Oceanic Eng. 15, 72–83.

Fichter, W., Pinson, M., 1989. Load-shortening behavior of an initially curved eccentrically loaded column. NASA Technical Memorandum 101643 42, 1–21.

Frisch-Fay, R., 1962. Flexible Bars. Washington, D C: Butterworth.

González, C., Lorca, J., 2004. Stiffness of a curved beam subjected to axial load and lardge displacements. Int. J. Solids Struct. 42, 1537–1545.

H.Evans, M., Fox, C., Lepora, N., Pearson, M., Sullivan, J., Prescott, T., 2014. The effect of whisker movement on radial distance estimation: a case study in comparative robotics. Active Touch Sens. 106, 108–118.

Love, A., 1892. A Treatise on the Mathematical Theory of Elasticity: Volume II. Cambridge University Press.

Pearson, M.J., A. G. Pipe, C.M., Mitchinson, B., Prescott, T.J., 2007. Whiskerbot: a robotic active touch system modeled on the rat whisker sensory system. Adapt. Behav. 15 (3), 223–240.

Quist, B., Hartmann, M., 2012. Mechanical signals at the base of a rat vibrissa: the effect of intrinsic vibrissa curvature and implications for tactile exploration. J. Neurophysiol. 9, 2298–2312.

Ramgulam, R.B., 2011. Modelling of knitting. In: Au, K. (Ed.), Advances in Knitting Technology. The Textile Institute: Woodhead Publishing, Oxford, pp. 48–85. chapter 4.

Snowdon, W., 1963. The bending of a thin rod having initial uniform curvature. Int. J. Mech. Sci. 5, 213–221.

Starostin, E., van der Heijden, G., 2009. Cascade unlooping of a low-pitch helical spring under tension. J. Mech. Phys. Solids 57, 959–969.